Journal of Materials Processing Technology 211 (2011) 1126–1135

Contents lists available at ScienceDirect

Journal of Materials Processing Technology

journal homepage: www.elsevier.com/locate/jmatprotec

Fatigue strength of tungsten inert gas-repaired weld joints in airplane critical structures

Marcelino P. Nascimento [a,*], Herman J.C. Voorwald [a], João da C. Payão Filho [b,1]

[a] State University of São Paulo, Department of Materials and Technology – UNESP/FEG/DMT, Av. Ariberto Pereira da Cunha, No. 333, CEP 12516-410, Guaratinguetá (SP), Brazil
[b] Federal University of Rio de Janeiro, Department of Metallurgical and Materials Engineering – PEMM/COPPE/UFRJ, Cidade Universitária, Centro de Tecnologia, Bloco F, Sala F-210, Ilha do Fundão, Caixa Postal 68505, CEP 21941-972, Rio de Janeiro (RJ), Brazil

ARTICLE INFO

Article history:
Received 23 March 2010
Received in revised form 9 January 2011
Accepted 18 January 2011
Available online 22 January 2011

Keywords:
AISI 4130 aeronautical steel
Repair welding
Weld metal and HAZ
Microstructure
Weld geometry
Flight-safety

ABSTRACT

In this work the effect of Gas Tungsten Arc Welding (GTAW) repairs on the axial fatigue strength of an AISI 4130 steel welded joint used in airframe critical to the flight-safety was investigated. Fatigue tests were performed at room temperature on 0.89 mm thick hot-rolled plates with constant amplitude and load ratio of $R = 0.1$, at 20 Hz frequency. Monotonic tensile tests, optical metallography and microhardness, residual stress and weld geometric factors measurements were also performed. The fatigue strength decreased with the number of GTAW repairs, and was related to microstructural and microhardness changes, as well as residual stress field and weld profile geometry factors, which gave origin to high stress concentration at the weld toe.

1. Introduction

Flight-safety has been the main area of concern for aeronautic authorities since the introduction of the first airplanes. One critical factor that aeronautical design must take into account is the difficulty of transporting load against gravity force during take-off and efficiently discharges it with minimum cost and maximum safety because failures in any of these stages can produce catastrophic accidents that often include loss of human lives (Godefroid, 1993). Since the catastrophic accidents with the English "Comet" airliner in the 1950s, the fatigue process has been the most important focus and operational consideration for both civil and military aircrafts (Goranson, 1993; Schijve, 2009). At present, in spite of the vast amount of experimental data generated in the last sixty years, fatigue failures still correspond to about 60% of the total failures in aircraft components (Findlay and Harrison, 2002; Bhaumik et al., 2008). This demonstrates the significance and complexity of the structural fatigue process and the importance of studying any aspects that would affect the frame structure of aircrafts.

Many fractures of aircraft materials are caused by fatigue as consequence of inadequate design and any kind of notch (stress concentrations) produced during manufacture or maintenance operations. Bhaumik et al. (2008) mentioned that failures in aircraft components can be due to a variety of reasons: (i) complex stress cycles, (ii) engineering design, (iii) manufacturing and inspection, (iv) service and environmental conditions, and (v) properties of the material. These authors also mentioned that the potential sources of fatigue failures can be related to one or more of the following errors: (i) design, (ii) manufacturing, (iii) assembly, (iv) inspection, (v) operation, and (vi) maintenance. In the same way, Goranson (1993), Wenner and Drury (2000) and Latorella and Prabhu (2000) mentioned that the structural failures during flight are usually attributed to fatigue of materials, design errors and aerodynamic overloads. Carpenter (2001) and Koski et al. (2006) further highlighted that due to the high number of older aircrafts that are flying nowadays, problems such as stress corrosion cracking, corrosion-fatigue (separately or simultaneously) and wear are also expected to occur. The understanding of all these issues demands extensive money and time investment, planning, research and development on maintenance and repair welding procedures toward assuring the safe and continued airworthiness of aircrafts.

The present study has helped demonstrate that the problem of fatigue failures is more complex and dangerous if an aircraft contains welded structures. Numerous difficulties that require con-

* Corresponding author. Tel.: +55 12 3123 2853; fax: +55 12 3123 2852.
E-mail addresses: marcelino.nascimento@gmail.com (M.P. Nascimento), voorwald@feg.unesp.br (H.J.C. Voorwald), jpayao@metalmat.ufrj.br (J.d.C. Payão Filho).
[1] Tel.: +55 21 2562 8500; fax: +55 21 2290 1615x233.

0924-0136/$ – see front matter © 2011 Elsevier B.V. All rights reserved.
doi:10.1016/j.jmatprotec.2011.01.016

sideration in evaluating and defining potential fatigue failures in welded structures have been determined as follows (Atzori et al., 2009):

- defining material properties which vary throughout the weld joint – weld metal (WM) and the heat affected zone (HAZ);
- presence of high residual stresses, both local (due to the weld itself) and structural (due to the assembly process of the structure) which also vary throughout the weld joint;
- defining precisely the weld bead geometry (bead size and shape) and radius at the toe of the weld, that vary even in well-controlled manufacturing and are the most important factors affecting the design and engineering of welded aircraft structures.

According to Aloraier et al. (2010), the weld toe cracking is caused by the weld metal that has higher yield strength and tensile strength than the parent metal (weld strength overmatch). These authors commented that "when the weld area shrinks on cooling from the welding temperature, cracking occurs in the heat-affected zone (HAZ) of the steel because the yield and strength levels of the HAZ are lower than those of the weld metal". Additionally, it is commented that "the toe region is highly susceptible to fatigue cracking due to the presence of weld defects, stress concentration due to toe geometry and adverse metallurgical conditions such as tensile residual stresses and coarse HAZ microstructure".

The presence of a tensile residual stress field and weld defects, such as slag inclusion at weld toe, undercut, lack of penetration and misalignment, is many times found in welded joints and effectively reduce the fatigue crack initiation phase. Wahab and Alam (2004) mentioned that the crack propagation stage was 75–89% of the total fatigue life for all types of welded joints tested, so that the entire life may be assumed to be dominated by crack propagation. These authors highlighted that in order to justify the integrity of welded structures, it is necessary to estimate the fatigue life of welded joints containing defects and to compare the obtained result with the required operational life that would be required for the aircraft.

In addition, welded aeronautic structures accumulate weld repairs which are carried out during the manufacturing and the operational life of aircraft. The size and frequency of defects depends on the welding process, welding procedure, geometry of the weld, ease of access to the place to be welded and care took during the welding (Wahab and Alam, 2004). In most cases, such defects are difficult and costly to detect and define nondestructively (Wahab and Alam, 2004). Repair welding is often carried out in situ with difficulty of access, without preheating and post weld heat treatment and without inspection (Lant et al., 2001).

Although efforts to improve the repair welding procedure for defective and degraded components have been extensive in the last decade, few papers have been written on this subject. Moreover, the great majority of them are about aged and degenerated metals in petrochemical and offshore industries and power plants (viz., Aloraier et al., 2010; Branza et al., 2009; Vega et al., 2008; Mirzaee-Sisan et al., 2007; Edwards et al., 2005; Lant et al., 2001). Additionally, most of the carried out studies are based on simulation by finite element method – FEM – (e.g., Sharples et al., 2005; Sun et al., 2005; Dong et al., 2005; Aloraier et al., 2004; Hyde et al., 2004). Consequently, there are only few studies about multiple repair welding operations (e.g., Vega et al., 2008).

Because repair welding is a necessary and frequently used procedure, one can conclude that the availability of experimental data about their effects on the structural integrity of aircrafts would be very important and useful. In this way, this would also help to determine effective inspection intervals of high-responsibility/critical components and to assess and assure the potential flight-safety of welded structures.

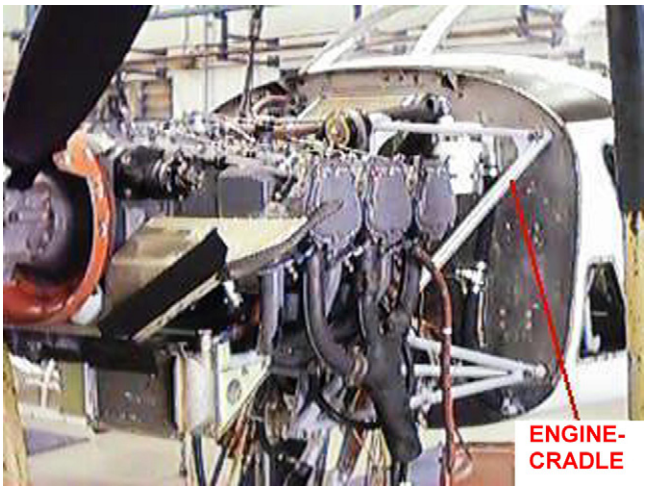

Fig. 1. Engine-cradle assembly in a Brazilian T-25 Universal aircraft.

In some aircraft models (e.g., agricultural, military training and acrobatic), the most repaired component is the one that supports the motor, called "engine-cradle" (Fig. 1). This component presents a geometrically complex structure made of AISI 4130 tubular steel of many different dimensions and TIG welded in several angles. In the Brazilian T-25 Universal aircraft, for example, besides supporting the motor at an extremity (correct balance), the engine-cradle also maintains the nose landing gear fixed at another extremity.

Because the engine-cradle is a component critical to flight-safety, the aeronautic standards are extremely rigorous in its manufacturing, imposing a "zero-defect index" to the quality of the welded joint. Consequently, this structure is 100% inspected by non-destructive testing (NDT). Importantly, these welded engine-cradle structures are frequently subjected to several repair welding operations during manufacture, so that they have to be in strict compliance to current standards ("zero-defect index"). As a consequence, even though approved by NDT during manufacture, these components may present a historic record of repair welding operations whose effects on the microstructure, mechanical properties and structural integrity are unknown.

This subject becomes even more complex when taking into account the additional historic record of repair welding operations during the service life of the aircraft (maintenance repair welding). For example, an investigation on 157 engine-cradle failure reports of Brazilian T-25 Universal aircrafts indicated that all failures occurred at welded joints as a result of fatigue cracks. As a consequence of these successive repair welding operations, the interval between inspections ("Time-Before-Fail") was reduced from 4000 h to 50 h of flight (Nascimento, 2004). Motivated by the high failure incidence on this component, an extensive research program to evaluate the effects of the repair welding on its structural integrity, mechanical properties and microstructure has been developed. The question that needed to be answered was: how many times can a welded joint be safely repaired by welding? The work described in this paper addressed the lack of data and analysis on this crucial subject.

Based on experimental results, the aim of this study was to investigate the effects of successive GTAW repairs on the axial fatigue strength of welded joints of AISI 4130 hot-rolled steel plates, 0.89 mm thick. Special emphasis was given to a commonly employed maintenance repair welding procedure, used during the operational life of aircrafts and characterized by overlapping the defective or fractured weld bead. The results obtained can contribute to an in-depth understanding on the subject as well as, to

Table 1
Chemical compositions (wt.%) specified for the base metal (BM) and the filler metal (FM) and analyzed of the BM and the weld metal (WM).

Composition (wt.%)	C	Mn	Si	$P_{Max.}$	$S_{Max.}$	Mo	Cr	Cu
Specified for the BM[a]	0.28–0.33	0.40–0.60	0.15–0.30	0.035	0.040	0.15–0.25	0.80–1.10	0.10
Analyzed of the BM	0.32	0.57	0.28	0.013	0.008	0.18	0.90	0.01
Specified for the FM[b]	0.28–0.33	0.40–0.60	0.15–0.35	0.008	0.008	0.15–0.25	0.80–1.10	0.10
Analyzed of the WM	0.30	0.50	0.25	0.004	0.003	0.18	0.91	0.042

[a] AMS T 6736 A (2003) – for chromium–molybdenum (4130) seamless and welded steel tubing of aircraft quality.
[b] AMS 6457 B – Turballoy 4130 Steel.

enable practical application of repair welding on aeronautic steel structures.

2. Materials and methods

2.1. Material

In the present work, flat butt welded specimens from hot-rolled AISI 4130 aeronautic steel, 0.89 mm (0.035-in.) thick, were used. The specified chemical compositions (wt.%) of the base metal (BM) and filler metal (FM) and the analyzed chemical compositions of the BM and weld metal (WM) are presented in Table 1 (Fe in balance). The average mechanical properties obtained from three smooth flat specimens of base metal and from three originally welded specimens (OR), with a central weld bead cross to the hot-rolled plate direction and to the applied tensile stress, are indicated in Table 2. The monotonic tensile tests were performed in accordance with ASTM E 8 M by means of a 100 kN-capacity Instron servo-hydraulic machine, with 0.5 mm/min displacement rate and a preload equal to 0.1 kN. The Rockwell hardness of the base metal was 65 HR_A.

2.2. Manufacturing welding and repair welding procedures

The most common welding process employed on manufacturing of aeronautical structures is the Gas Tungsten Arc Welding (GTAW), or Tungsten Inert Gas (TIG), which is appropriate to weld thin metals by allowing the control of the main variables and by resulting in high-quality and defect-free welded joints. The manufacturing welding and the repair welding were carried out in accordance with the Embraer NE-40-056 Type 1 Standard (for components critical to the flight-safety), as specified by the Brazilian aeronautic industry, with 99.95% purity argon as shielding gas and with AMS 6457 B – Turballoy 4130 filler metal. The joints were manually welded by a skilled aeronautic welder using a Square Wave TIG 355 Lincoln power source. The main welding parameters used to make the welds are given in Table 3. All welded joints were X-ray inspected by the Brazilian Aerospace Technical Centre (CTA/IFI), which approved them in accordance with the MIL-STD-453, the Embraer NE-57-002 and the ASTM E-390 standards.

The welding direction was always perpendicular to the hot-rolling direction of the plate. Before welding, samples were cleaned with chlorinated solvent to ensure oxide removal and fixed on a backing bar to avoid contamination and porosity in the weld root. In order to reproduce the actual manufacture welding procedure of aeronautic structures, no subsequent stress relieves heat treatment was carried out on the welded joints. Because of the 0.89 mm thick of the base metal, only a single weld pass was required. The repair welding was carried out by overlapping the weld seam, i.e., without removing the previous weld bead. Fig. 2 schematically illustrates the repair welding procedure by overlapping the fractured weld bead, which is commonly used on aircraft structures during their operational life (maintenance welding). This maintenance welding procedure can be used in case of emergency or when the removal of a defective weld seam is uneconomical, impractical or impossible. In according with the number of repair welds, the specimens were identified as OR (original weld, i.e., manufacturing weld), 1R (with one repair weld) and 2R (with two repair welds). The weld-

Table 3
Gas Tungsten Arc Welding (GTAW) parameters.

Welding position	Flat
Type of current and polarity	DCEN
Welding current, I	40 A
Welding voltage, U	12 V
Welding speed, V	18.0 cm min^{-1}
Heat input, HI[a]	1.1 kJ cm^{-1}
Preheating temperature	No
Shielding gas flow rate	5 L min^{-1}
Filler metal diameter	1.6 mm

[a] $HI = \eta \times (U \times I)/V$; η = heat source efficiency (70%).

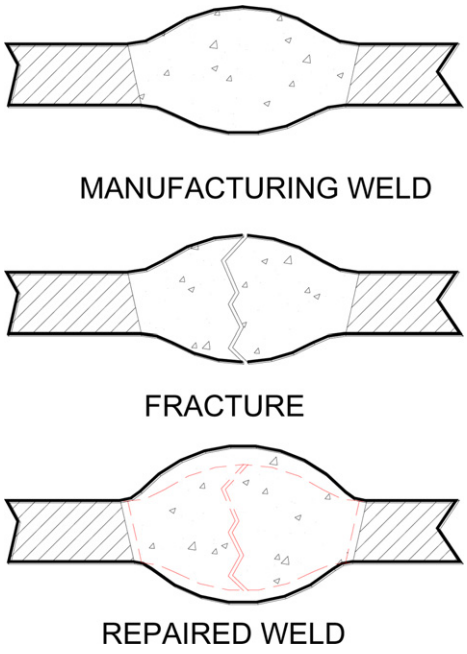

Fig. 2. Repair welding procedure by overlapping the previous weld bead.

Table 2
Mechanical properties of the base metal (BM) and of the originally welded specimen (OR).

Specimen	Yield strength (0.2% offset) [MPa]	Tensile strength [MPa]	Rupture stress [MPa]	Elongation (25 mm length) [%]	Yield strength/tensile strength ratio
BM	740 ± 2	809 ± 3	669 ± 11	8.48 ± 1.00	0.91 ± 0.00
OR	671 ± 20	778 ± 17	643 ± 26	3.81 ± 0.26	0.86 ± 0.01

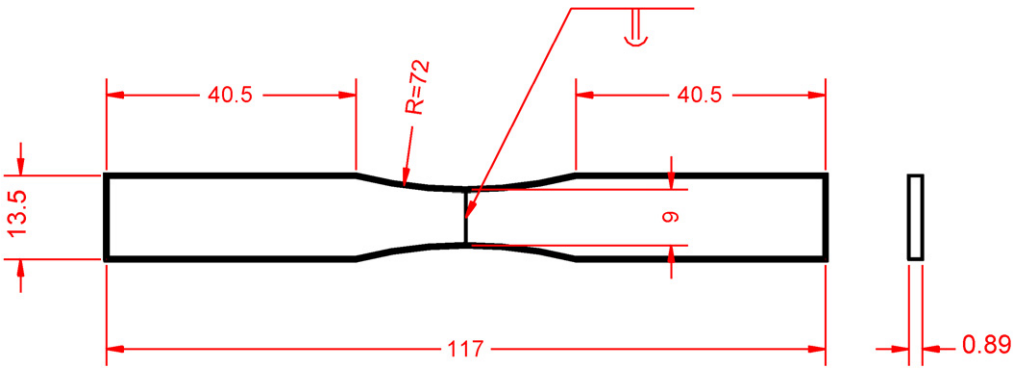

Fig. 3. Flat axial fatigue specimen, with dimensions in [mm].

ing parameters used, and consequently the heat input, were kept constant for all the conditions.

2.3. Axial fatigue tests

For axial fatigue experimental tests, specimens were manufactured in accordance with the ASTM E 466 requirements (Fig. 3), following the LT direction of the hot-rolled plate.

The specimens were fatigue tested in a 100 kN-capacity Instron servo-hydraulic machine with a sinusoidal constant amplitude load, stress ratio $R = 0.1$, at 20 Hz frequency and at room temperature. The superficial average roughness, obtained by means of a Mitutoyo 301 equipment with cut-off equal to 0.8 mm × 5 mm, was $R_a = 0.73 \pm 0.12$ μm.

2.4. Microstructural analysis and microhardness

For microstructural analysis, specimens were grinded, mechanically polished and chemically etched with Nital 2% during 5 s. The grain size of the heat affected zone of the base metal immediately adjacent to the weld metal (coarse grain heat affected zone – CGHAZ) was measured in accordance with the intercept method described in the ASTM E 112-96 (Standard Test Methods for Determining Average Grain Size). The grain boundaries were revealed by etching chemically the CGHAZ during 40 s with a solution of 2 g of ferric chloride and 2 g of picric acid in distilled water. Vickers microhardness measurements with 1 N load were obtained at 0.0254 mm intervals throughout the regions under analysis (BM, HAZ and WM).

2.5. Residual stresses determination

The residual stresses field induced by the original and by the repair welding was determined by X-ray diffraction method using the Raystress equipment developed by Ivanov et al. (1994), with couple exhibition, φ goniometer geometer, two anodes of chrome Cr Kα radiation and registration of {2 2 1} diffraction lines. Additionally, a 25 kV power supply, current of 1.5 mA and X-ray convergence angle of 50° was employed. The accuracy of the stress measurements was $\Delta\sigma = \pm 20$ MPa. In order to obtain the stress distribution by depth, the specimen superficial layers were removed by electrolytic polishing with an acid solution.

3. Results

3.1. Monotonic tensile tests

Table 2 presents the mechanical properties of the hot-rolled AISI 4130 steel plate with and without the central weld bead, as well as the yield strength/tensile stress ratio (σ_y/σ_m). Historically, values from 0.80 to 0.86 have been considered appropriate for specification, project and analysis of structural integrity, by providing high capacity of plastic deformation and consequent margin of safety against fracture (Bannister et al., 2000). Fig. 4 presents some monotonically fractured tensile welded specimens.

3.2. Axial fatigue tests

Fig. 5 presents the SN (stress vs. number of cycles) curves for the base metal, original welded and repair welded specimens. The horizontal dashed line indicates the nominal stress value ($\sigma_n \approx 247$ MPa), which corresponds to yield strength divided by the safety-factor equal to 3, as requested by Embraer NE 40-056 Type 1 Standard (for welded components critical to flight-safety).

The axial fatigue strength results obtained can be more precisely analyzed from Fig. 6, which depicts the linear regressions (stress vs. the number of cycles, $\log N$) of the curves illustrated in Fig. 5.

3.2.1. Vickers microhardness (HV)

Fig. 7 presents the Vickers microhardness of the three interest zones of the welded joints. Firstly, one can observe the high Vickers microhardness values of the WM, CGHAZ and FGHAZ (fine grain HAZ).

The Vickers microhardness of the specimens 1R and 2R are in accordance with Eq. (1), proposed by Yurioka (1987) to determine the martensite hardness (H_M) in HAZ as a function of the carbon

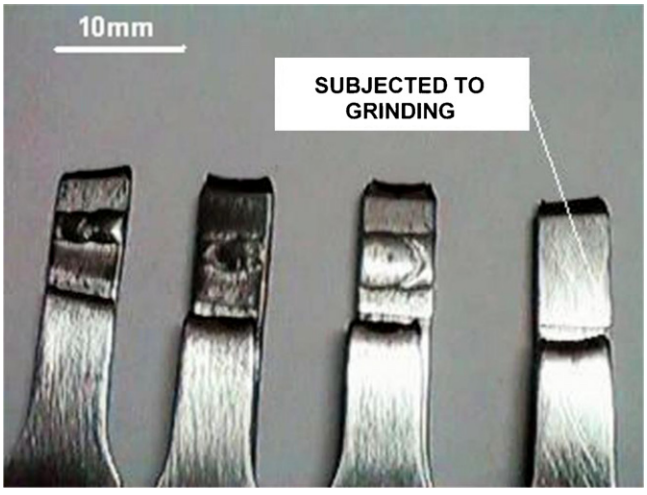

Fig. 4. Specimens fractured by monotonic tensile tests. Tensile specimens fractured at the subcritical heat affected zone (SCHAZ) of the welded joints immediately under its intercritical heat affected zone (ICHAZ).

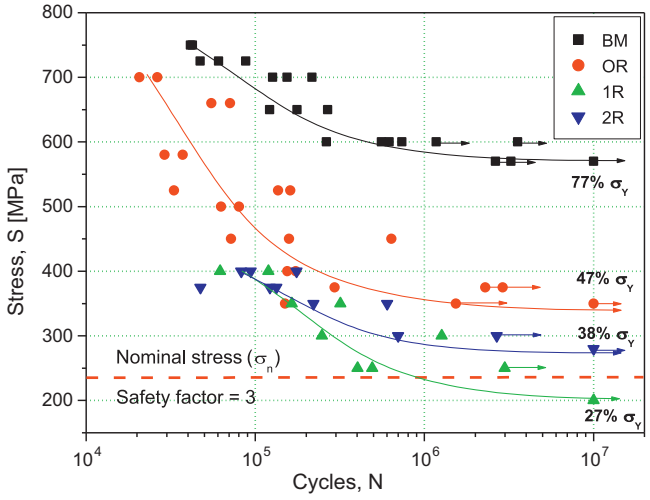

Fig. 5. SN (stress vs. number of cycles) axial fatigue strength curves of the base metal (BM) and original (OR), one repair (1R) and two repairs (2R) welded joints.

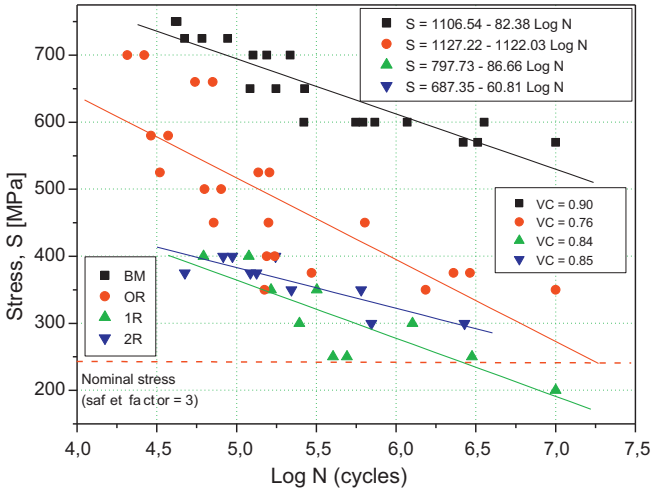

Fig. 6. Linear regression of the fatigue strength curves presented in this figure, where VC = variation coefficient, BM = base metal, OR = original weld, 1R = one repair welded joint and 2R = two repairs welded joints.

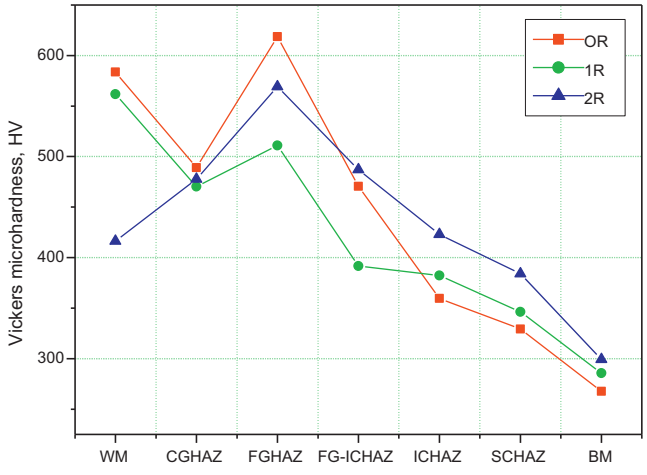

Fig. 7. Vickers microhardness of the different regions of the original (OR), one repair (1R) and two repairs (2R) welded joints. Where, WM = weld metal, CGHAZ = coarse grain heat affected zone, FGHAZ = fine grain heat affected zone, FG-ICHAZ = fine grain to intercritical heat affected zone transition, ICHAZ = intercritical heat affected zone, SCHAZ = subcritical heat affected zone and BM = base metal.

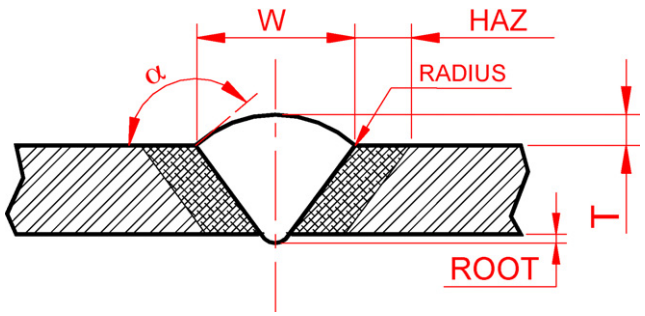

Fig. 8. Main weld joint geometric factors (data presented in Table 4), where "*W*" is the weld width, "*α*" is the angle between the weld and the base metal, "HAZ" is the heat affected zone, "*T*" is the weld reinforcement and "*R*" is the weld root reinforcement.

content (percentage in weight) of the steel:

$$H_M = 884 \times \%C \times (1 - 0.3 \times \%C^2) + 294 \quad (1)$$

Application of the Yurioka's equation resulted in 568 HV.

3.2.2. Weld geometry factors

Fig. 8 and Table 4 present the values of the main geometry factors of the welded joints, obtained by image analysis software.

Since the weld geometry affects the fatigue strength of a welded structure and that the weld toe is the zone of the welded joint most critical to the fatigue process, based on results presented in Table 4. Fig. 9 depicts the angle α vs. the radius of the weld toe notch for both original and repair welded specimens. It is important to say, however, that the angle α and the radius at the weld toe can change along the length of the weld seam.

Fig. 10 shows a scanning electron microscopy (SEM) of the fracture surface of a welded specimen, whose fatigue crack initiated at the weld toe.

3.2.3. Microstructure analysis

Fig. 11 presents the BM and HAZ (ICHAZ and SCHAZ) microstructures, obtained by optical microscopy of the manufacturing welded joint. The BM grain size was 32 μm.

Fig. 12 shows the microstructures in the CGHAZ and WM of the OR, 1R and 2R welded joints, which are formed by martensite. The CGHAZ grain sizes of the OR and 1R welded joints were 88 μm; of the 2R, 123 μm.

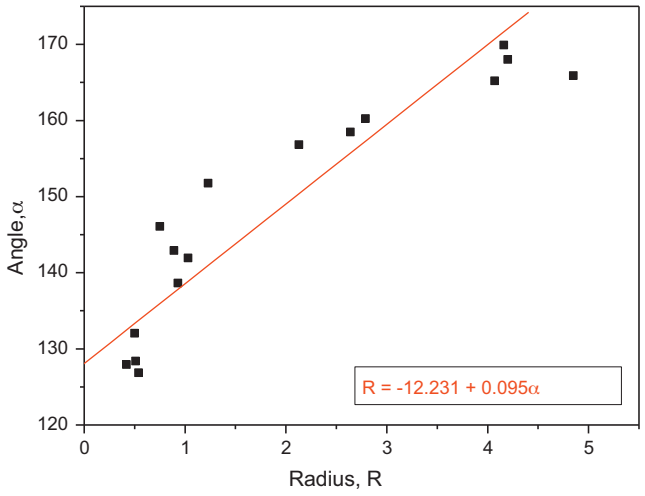

Fig. 9. Relationship between the radius (*R*) and the angle (*α*) at the weld toe of the joints (data presented in Table 4) and its linear regression.

Table 4
Geometric factors of the weld bead of all the specimens tested.

Group	W [mm]	T [mm]	Root R [mm]	Angle α [°]	Radius r [mm]	HAZ size [mm]	K_t (Eq. (3))
OR	3.97 ± 0.58	0.54 ± 0.19	0.41 ± 0.17	142.91 ± 14.32	0.89 ± 1.09	3.01 ± 0.57	1.676
1R	5.36 ± 0.70	1.17 ± 0.28	0.65 ± 0.24	127.93 ± 14.02	0.42 ± 0.16	4.72 ± 0.34	3.443
2R	5.10 ± 0.64	1.27 ± 0.14	0.69 ± 0.10	126.87 ± 14.39	0.54 ± 0.44	5.02 ± 0.39	2.310

W = weld bead width; T = weld reinforcement; R = root reinforcement; α = angle between the weld and the base metal; r = radius of the weld toe notch; HAZ = heat affected zone.

$$K_f = 1 + \frac{K_t - 1}{1 + a/r} \quad (3)$$

a = 0.1659 (Peterson's parameter for steel); K_f = fatigue-notch factor; K_t = stress concentration factor.

3.2.4. Residual stresses

Fig. 13 presents the residual stresses profile in the welded joints (WM, HAZ and BM). One can observe in Fig. 13 that the original and the repair welding have introduced high compressive residual stresses in all the joints. It is also possible to observe in this figure that all the residual stress profiles presented similar tendency, i.e., maximum values in the weld metals (−600 MPa for OR, −460 MPa for 1R and −340 MPa for 2R), followed by the HAZ (−410 MPa for OR, −80 MPa for 1R and −50 MPa for 2R) and the base metals, 20 mm away from the fusion line (−330 MPa for OR, −110 MPa for 1R and −160 MPa for 2R). Fig. 13 also shows that the second repair welding relieved the compressive stress fields generated by the original welding and the first repair welding. The residual stress fields were relieved internally beyond 20 mm away from the weld metal (fusion line) because there was no deformation on the samples.

4. Discussion

4.1. Monotonic tensile tests

From Table 2, it is important to note the high mechanical strength values and reasonable ductility of the hot-rolled AISI 4130 steel plate. Here one can also observe the decrease of all the mechanical properties with the GTAW of AISI 4130 steel joints, particularly the elongation, which reached a very low value (3.8% average), typical of brittle material. Nevertheless, the yield strength/tensile strength ratio (σ_y/σ_m) decreased from 0.91 for the base metal to 0.86 after the original welding, which is an appropriate value for structural components. From Fig. 4, one can also observe that all the monotonic tensile specimens tested, including the one subjected to grinding, fractured in the subcritical heat affected zone (SCHAZ), i.e., in base metal non-affected by the welding heat just below the intercritical heat affected zone (ICHAZ), due to the weld strength overmatch. This means that the microstructural changes in the HAZ were more important to the fracture process than the stress concentration introduced by the geometric factors of the weld. Thus, for the monotonic tensile tests, the AISI 4130 steel was not sensitive to stress concentration at the weld toe notch.

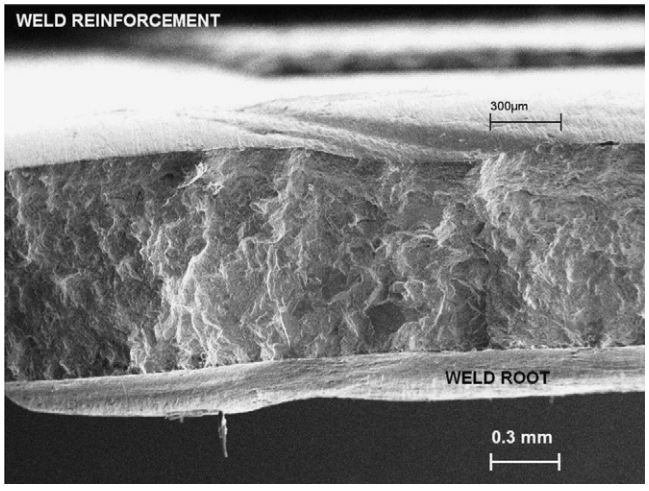

Fig. 10. Scanning electron microscopy of the fracture surface of a welded joint, whose fatigue crack began at the weld toe.

4.2. Axial fatigue tests

From Fig. 5, one can observe the good behavior of the AISI 4130 steel subjected to axial fatigue, where the endurance limit was about 77% of its yield strength (σ_y) and above the nominal stress, σ_n (dashed line). It was also observed the smaller axial fatigue strength of the butt welded specimens than those of the base metal, for both low ($<10^5$) and high ($>10^5$) fatigue cycles (in this paper called LFC and HFC, respectively), whose endurance limit was about 47% of the yield strength of the base metal. Nevertheless, the endurance limit is also located above σ_n in the HFC range. The fatigue behavior presented in Fig. 5 is associated with very low elongation value (3.81% average) obtained from the monotonic tensile tests aforementioned.

A subsequent reduction of the axial fatigue strength with the first repair welding (1R) is observed in Fig. 5, with the endurance limit crossing down the σ_n in the HFC range. The second repair welding (2R) produced discreet recovery of the axial fatigue strength, but with the endurance limit close to the σ_n. After the repair welding (1R and 2R), the greater weld volume increases the cooling rate of the weld joint (weld metal and coarse grain heat affected zone – CGHAZ), promoting the formation of martensite at the weld toe.

It is also possible to verify in Fig. 5 the large scatter of the axial fatigue strength values of the original and repair welded specimens. This is due to the different volumes of weld metals, which affects the cooling rate of the welded joints, the microstructure and the stress concentration at the weld toe. Moreover, it is also possible to verify the convergence of 1R and 2R fatigue curves in the LFC range ($<10^5$ cycles), witch results in K_f (fatigue-notch factor) tending to unit ($K_f = 1$). In this case, even if K_t (theoretical stress concentration factor) is high ($\gg 1$), the notch-sensitivity factor (q), described in Eq. (2), will be equal to zero in LFC:

$$q = \left(\frac{K_f - 1}{K_t - 1} \right) \quad (2)$$

From Fig. 6, one can also clearly verify the accentuated decrease of the axial fatigue strength of the original welded and repair welded joints. The equations of linear regression presented in Fig. 6 indicate the follow variation coefficients (R): 90% for BM, 76% for OR, 84% for 1R and 85% for 2R.

In addition to the above discussed results, one can say that the increase of the weld volume with the number of weld repairs increased size of the HAZ, particularly the coarse grain heat affected

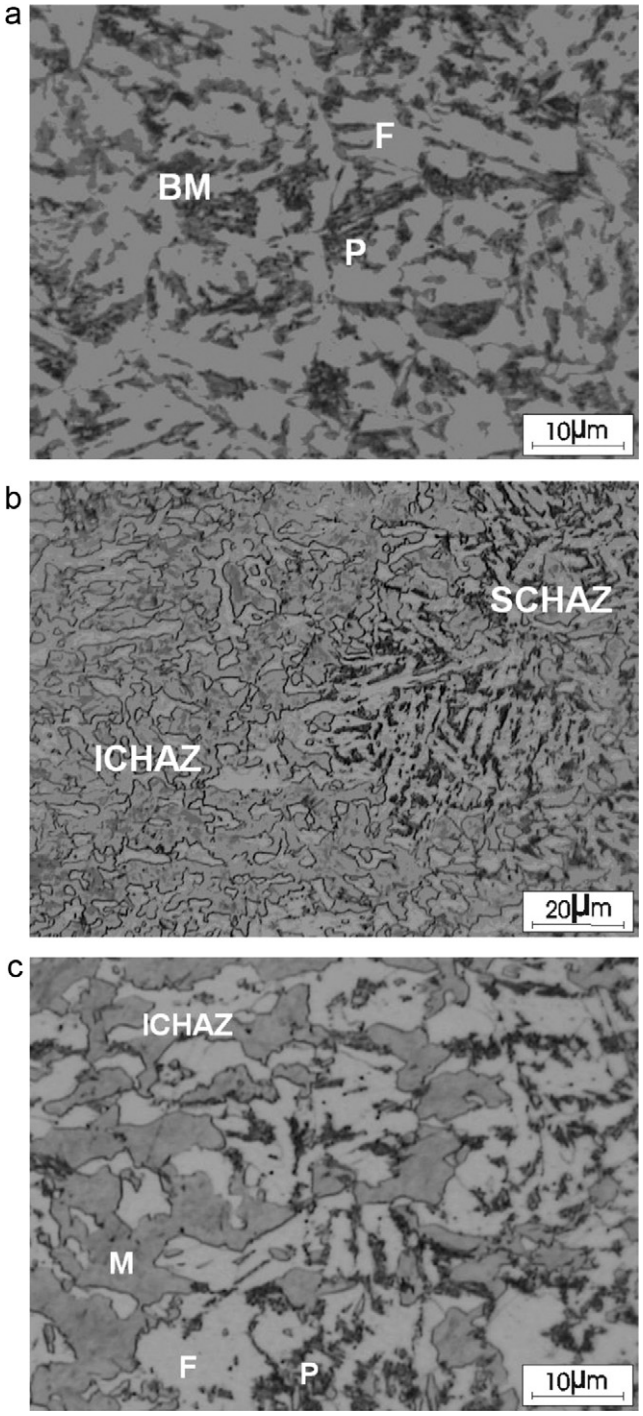

Fig. 11. Microstructures of the base metal (BM) and of the heat affected zone (HAZ) of the original welded joint: (a) BM with fine grain ferrite (F) and pearlite (P); (b) and (c) transition of the intercritical to the subcritical heat affected zone (ICHAZ and SCHAZ, respectively), showing the formation of martensite (M) and fine grain ferrite and pearlite. Optical microscopy. Nital 2%.

zone, which is characterized by low fracture toughness and considerable hardness (as can be seen in Fig. 7). The original and repair welded specimens fractured in the WM/CGHAZ interface (fusion line), so that it can be inferred that the repair welding strongly increases the susceptibility to structural integrity degradation of this particular high-responsibility component. Because aircrafts are subjected to high fatigue cycles during flight (due to abrupt maneuvers, wind bursts, motor vibration and helixes efforts), it is recommended to the flight-safety no repair welding during the operational life of aircrafts. However, if repairs are necessary, care should be taken toward avoiding abrupt maneuvers during flight and/or overloads on the aircraft. In this case, it is necessary to decrease the intervals between inspections for crack-like flaws in welded joints.

4.3. Vickers microhardness

The high Vickers microhardness values presented in Fig. 7 are due to the low heat input of the welding, and consequent high cooling rate of the welded joints, as well as to the chemical composition of the WM and BM, which promotes the formation of martensite. Since the heat input was constant for all the welding conditions, the scatter of the Vickers microhardness in the WM was due to the overlapping of the weld metal to the previous weld bead, resulting greater weld metal volume and consequently higher cooling rates with the repair cycles.

It can be seen in Fig. 7 that the Vickers microhardness values in the CGHAZ, which is the most critical to the fatigue process, are close with each other. Moreover, one can observe the increase of the Vickers microhardness from the CGHAZ to FGHAZ and its subsequent decreasing to the base metal, as expected (the higher the grain size, the lower the mechanical strength and the hardness). The second repair welding decreases the Vickers microhardness of the WM, CGHAZ and FGHAZ due to the coarser grain size. It is well established that grain refining can improve at the same time the yield strength and the toughness and hardness of metals. This improvement can be quantified in a constitutive relation known as Hall–Petch relation. The second repair of the manufacturing welded joint has effectively increased the gain size of the coarse grain heat affected zone, in accordance with the results presented in Section 3.2.3. The increase of the grain size in the CGHAZ induced toughness loss in this zone and lowered consequently its axial fatigue strength.

4.4. Weld geometry factors

From Fig. 8 and Table 4, it can be observed that the repair welding reduced both the angle α and the radius of the weld toe notch, consequently increasing the local stress concentration factor (K_t). From the data of Table 4 and Fig. 9 highlights the inter-relation between the angle α and the radius at the weld toe, which are recognized as the most important factors for the fatigue strength of welded joints, as described by Lancaster (1993) and Aloraier et al. (2010). That is: the smaller the angle α and the radius of the weld toe notch, the smaller is the fatigue strength (higher K_t). It can explicate the smaller fatigue strength of the 1R specimens in comparison with the 2R specimens (Figs. 5 and 6).

In a previous study, Wahab and Alam (2004) mentioned that the stress intensity factor is strongly influenced by the weld profile geometry factors and that the majority of fatigue cracks in welded structures originate at the weld toe or at the weld end rather than at internal defects. In the present research work, all the fatigue specimens also fractured at the WM/CGHAZ interface (fusion line or weld toe), as can be seen in Fig. 10.

From Table 4, one can also observe:

i. the increase of the Peterson (1997) stress concentration factor, K_t (Eq. (3)), at the weld toe notch with the successive repair welding operations (higher for the first repair welding, followed by the second one and them by the original welding), is in accordance with the axial fatigue strength presented in Fig. 5;
ii. the greater size of the HAZ and, consequently, of the CGHAZ;
iii. the relationship between the weld metal and root reinforcements (T and R, respectively) and the angle α and radius of the weld toe and, consequently, the axial fatigue strength (Fig. 5).

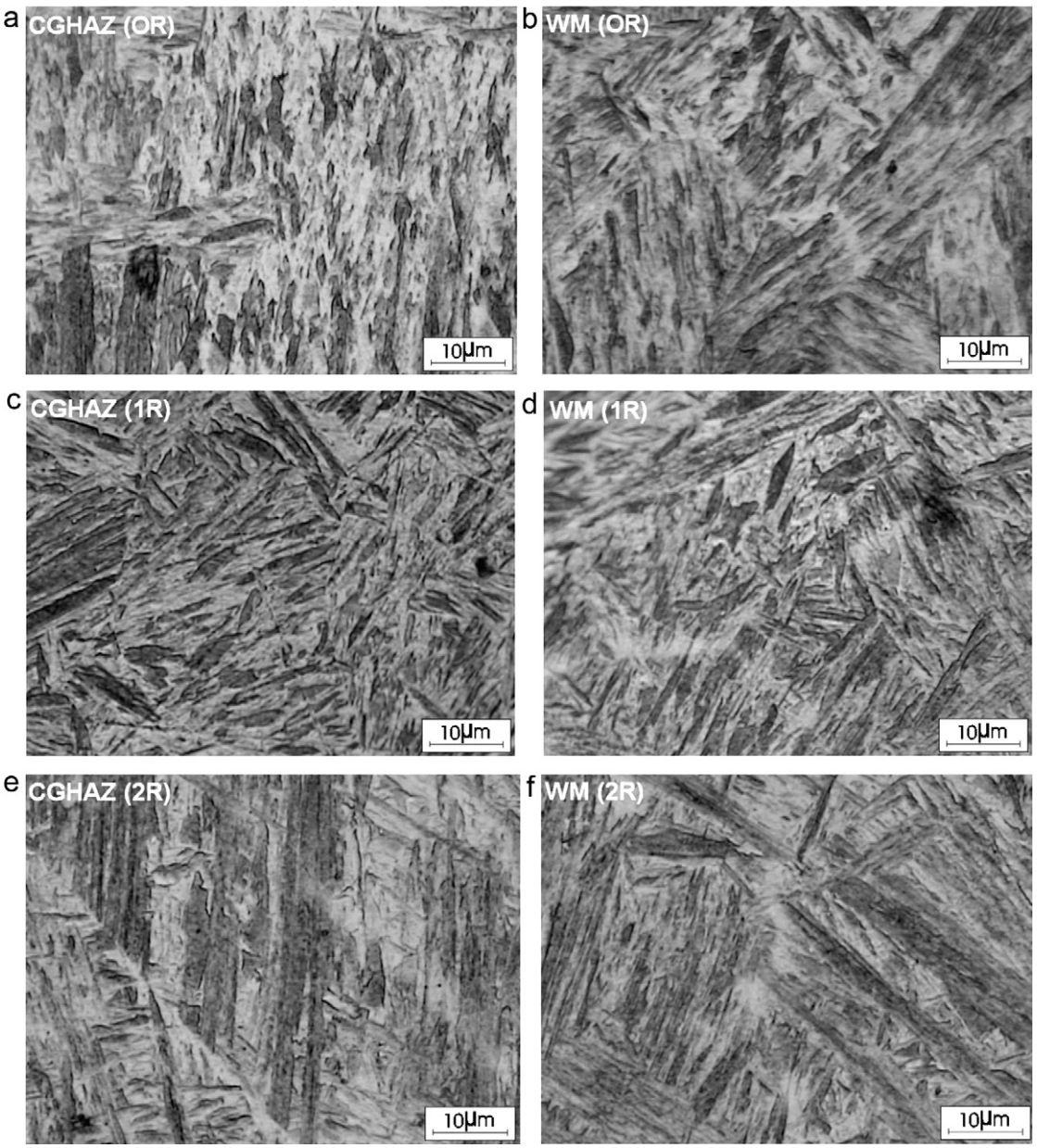

Fig. 12. Microstructures of the coarse grain heat affected zone (CGHAZ) and weld metal (WM) of the original welded joint (OR), one repair welded joint (1R) and two repairs welded joint (2R). Optical microscopy. Nital 2%.

Finally, it can also be observed in Table 4 that the scatter of weld geometry factors is in accordance with the great scatter of the axial fatigue strength depicted in Fig. 5.

4.5. Microstructure analysis

Fig. 11(a) shows the microstructure of the base metal (an AISI 4130 hot-rolled normalized steel). The white areas are fine grain primary ferrite (F); the grey ones, a mixture of two phases (ferrite and cementite) known as fine pearlite (P). Fig. 11(b) illustrates the microstructure formed near the A_1 isothermal (temperature at witch the pearlite transforms to austenite on heating) of the HAZ of a welded joint. The region of the HAZ heated during the welding just above A_1 is called intercritical heat affected zone; the one heated just below A_1, sub-critical heat affected zone. Fig. 11(c) shows with higher magnification the ICHAZ–SCHAZ transition. The white areas are ferrite (F); the light grey, martensite (M); and the dark grey, pearlite (P). The austenite transformed from pearlite in the ICHAZ on heating during the welding, originates martensite on cooling due to its high carbon content (≅0.78%C) and to the high cooling rates of the welded joints.

The microstructure of the CGHAZ and WM of the welded joints (OR, 1R and 2R) is 100% coarse grain martensite, a hard and brittle constituent (Fig. 12). As aforementioned, the higher the hardness of the microstructure, the higher its resistance to fatigue crack nucleation. On the other hand, it is well known that crack initiation usually will be faster in coarse grain microstructures (Ravi et al., 2004).

4.6. Residual stresses

Studies carried out by Dong et al. (2005), Wei and Chen (1994), Brown et al. (2006) and Chiarelli et al. (1999) revealed that residual stresses are unavoidably present in welded components.

From Fig. 13, some points are worth to be mentioned: the high compressive residual stresses, which were higher in the weld metal

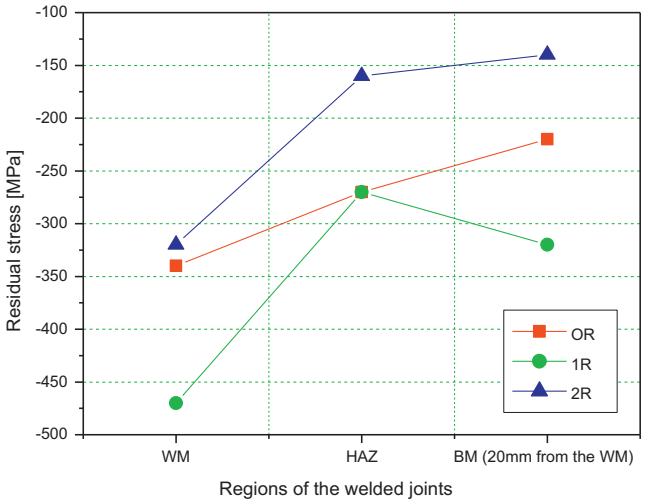

Fig. 13. Residual stress in the base metal (BM), 20 mm far from the weld metal (WM), and in the heat affected zone (HAZ) and WM of the original (OR), one repair (1R) and two repairs (2R) welded joints.

than HAZ; and the residual compressive stress field, up to 20 mm far away from the weld metal (fusion line). It is well known that residual stresses largely affect the fatigue strength of any components carrying load (Broek, 1991; Suresh, 1998) and that compressive residual stresses are beneficial toward inhibiting the crack nucleation. That means, the higher the hardness of the microstructure, the higher its resistance to the fatigue crack nucleation. On the other hand, it is also well known that the higher the hardness the higher the crack propagation rate, da/dN (Anderson, 1995; Broek, 1991; Suresh, 1998).

One factor which might have contributed to the compressive residual stresses induced by the GTAW (presented in Fig. 13) is the austenite–martensite transformation, which generates up to 4% increase in volume of material.

Furthermore, it is possible to infer that the compressive residual stress benefits were minimized or relieve by a local tensile stress concentration capable to reduce the number of cycles necessary to initiate fatigue crack. That is, it is possible that the geometric stress concentration factor at the weld toe has counteracted the compressive residual stress field induced by the repair welding. Moreover, the compressive residual stresses field, as far as possible, certainly delayed the fatigue crack nucleation and propagation by reducing the stress intensity factor (ΔK), as mentioned by Wei and Chen (1994).

5. Conclusions

Motivated by high fracture incidence at AISI 4130 steel welded joints of a specific component critical to the flight-safety, called "engine-cradle", experimental axial fatigue tests on manufacturing welded and repair welded specimens were carried out. Based on the results obtained, the following conclusions may be drawn:

- the GTAW decreased all the mechanical properties of the AISI 4130 steel, particularly the ductility;
- the GTAW reduced the axial fatigue strength of the AISI steel, but it was still above the nominal stress specified by the Brazilian aeronautic standard;
- the first repair welding reduced the axial fatigue strength of the manufacturing welded joint; the second one, recovered it a little bit;
- the axial fatigue strength of the repair welded joints was largely affected by the microstructure (coarse grain martensite) and the microhardness of the CGHAZ and, mostly, by the geometry factors at the welded joints, particularly the angle α and radius of the weld toe;
- the high local stress concentration (K_t), associated to the angle α and radius of the weld toe, relieved and/or overcomes the compressive residual stress field originated by the TIG welding process.

Acknowledgment

The authors are grateful to Fapesp (process no. 99/11948-6), CNPq and Fundunesp.

References

Aloraier, A.S., Ibrahim, R.N., Ghojet, J., 2004. Eliminating post-weld heat treatment in repair welding by temper bead technique: role bead sequence in metallurgical changes. Journal of Materials Processing Technology 153–154, 392–400.
Aloraier, A., Al-Mazrouee, A., Price, J.W.H., Shehata, T., 2010. Weld repair practices without post weld heat treatment for ferritic alloys and their consequences on residual stresses: a review. International Journal of Pressure Vessels and Piping 87, 127–133.
Anderson, T.L., 1995. Fracture Mechanics: Fundaments and Applications, 2nd ed. CRC Press, New York.
Atzori, B., Lazzarin, P., Meneghetti, G., Ricotta, M., 2009. Fatigue design of complex welded structures. International Journal of Fatigue 31, 59–69.
Bannister, A.C., Ocejo, J.R., Gutierrez-Solana, F., 2000. Implications of the yield stress/tensile stress ratio to the SINTAP failure assessment diagrams for homogeneous materials. Engineering Fracture Mechanics 67, 547–562.
Bhaumik, S.K., Sujata, M., Venkataswamy, M.A., 2008. Fatigue failure of aircraft components. Engineering Failure Analysis 15, 675–694.
Branza, T., Deschaux-Beaume, F., Sierra, G., Lours, P., 2009. Study and prevention of cracking during weld-repair of heat-resistant cast steels. Journal of Materials Processing Technology 209, 536–547.
Broek, D., 1991. The Practical Use of Fracture Mechanics, 3rd ed. Kluwer Academic Publishers, OH, USA, pp. 522.
Brown, T.B., Dauda, T.A., Truman, C.E., Smith, D.J., Memhard, D., Pfeiffer, W., 2006. Predictions and measurements of residual stress in repair welds in plates. International Journal of Pressure Vessels and Piping 83, 809–818.
Carpenter, M., 2001. Managing the fleet: materials degradation and its effect on aging aircraft. The Amptiac. News Letter 4 (5), 7–19.
Chiarelli, M., Lanciotti, A., Sacchi, M., 1999. Fatigue resistance of MAG welded steel elements. International Journal of Fatigue 1, 1099–1110.
Dong, P., Hong, J.K., Bouchard, P.J., 2005. Analysis of residual stresses at weld repairs. International Journal of Pressure Vessels and Piping 82, 258–269.
Edwards, L., Bouchard, P.J., Dutta, M., Wang, D.Q., Santisteban, J.R., Hiller, S., Fitzpatrick, M.E., 2005. Direct measurement of the residual stresses near a 'boat-shaped' repair in a 20 mm thick stainless steel tube butt weld. International Journal of Pressure Vessels and Piping 82, 288–298.
Findlay, S.J., Harrison, N.D., 2002. Why aircraft fail? Materials Today (November), 18–25.
Godefroid, L.B., 1993. Fatigue crack growth under constant and variable amplitude loading in aluminum alloys of aeronautical applications, Ph.D. Thesis, COPPE, Federal University of Rio de Janeiro, Brazil.
Goranson, U.G., 1993. Fatigue issues in aircraft maintenance and repairs. International Journal of Fatigue 19, S3–S21.
Hyde, T.H., Sun, W., Becker, A.A., Williams, J.A., 2004. Life prediction of repaired welds in a pressurized CrMoV pipe with incorporation of initial damage. International Journal of Pressure Vessels and Piping 81, 1–12.
Ivanov, S.A., Monim, V.I., Teodósio, J.R., 1994. New method of X-ray tensiometry. In: Proceedings of International Conference on Experimental Mechanics , Lisbon, Portugal, pp. 757–761.
Koski, K., Tikka, J., Bäckström, M., Siljander, A., Liukkonen, S., Marquis, G., 2006. An aging aircraft's wing under complex multiaxial spectrum loading: fatigue assessment and repairing. International Journal of Fatigue 28, 652–656.
Lancaster, J.F., 1993. Metallurgy of Welding, 5th ed. Chapman & Hall Incorporation, London, pp. 164–258.
Lant, T., Robinson, D.L., Spafford, B., Storesund, J., 2001. Review of weld repair procedures for low alloy steels design minimize the risk of future cracking. International Journal of Pressure Vessel and Piping 78, 813–818.
Latorella, K.A., Prabhu, P.V., 2000. A review of human error in aviation maintenance and inspection. International Journal of Industrial Ergonomics 26, 133–161.
Mirzaee-Sisan, A., Fookes, A.J., Truman, C.E., Smith, D.J., Brown, T.B., Dauda, T.A., 2007. Residual stress measurement in a repair welded header in the as-welded condition and after advanced post weld treatment. International Journal of Pressure Vessels and Piping 84, 265–273.
Nascimento, M.P., 2004. Effects of TIG welding repair on the structural integrity of AISI 4130 aeronautical steel. Ph.D. Thesis in Mechanical Engineering. State University of São Paulo/UNESP-FEG, Brazil (in Portuguese), Code CDU 620.92, 240 p.

Peterson, R.E., 1997. Stress Concentration Design Factors, 2nd ed. John Wiley & Sons Incorporation, New York, pp. 151.
Ravi, S., Balasubramanian, V., Babu, S., Nasser, S.N., 2004. Influences of MMR, PWHT and notch location on fatigue life of HSLA steel welds. Engineering Failure Analysis 11, 619–634.
Schijve, J., 2009. Fatigue damage in aircraft structures, not wanted, but tolerated? International Journal of Fatigue 31, 998–1011.
Sharples, J.K., Gardner, L., Bate, S.K., Goldthorpe, M.R., Yates, J.R., Bainbridge, H., 2005. (FEM) Project to evaluate the integrity of repaired welds. International Journal of Pressure Vessels and Piping 82, 319–338.
Sun, W., Hyde, T.H., Becker, A.A., Williams, J.A., 2005. Some key effects on the failure assessment of weld repairs in CrMoV pipelines using continuum damage modeling. Engineering Failure Analysis 12, 839–850.
Suresh, S., 1998. Fatigue of Materials, 2nd ed. Cambridge University Press, London, pp. 1–679.
Vega, O.E., Hallen, J.M., Villagomez, A., Contreras, A., 2008. Effect of multiple repairs in girth welds of pipelines on the mechanical properties. Materials Characterization 59, 1498–1507.
Wahab, M.A., Alam, M.S., 2004. The significance of weld imperfections and surface peening on fatigue crack propagation life of butt-welded joints. Journal of Materials Processing Technology 153–154, 931–937.
Wei, M.Y., Chen, C., 1994. Fatigue crack growth characteristics of laser-hardened 4130 steel. Scripta Metallurgica et Materialia 10 (31), 1393–1398.
Wenner, C.A., Drury, C.G., 2000. Analyzing human error in aircraft ground damage incidents. International Journal of Industrial Ergonomics 26, 177–199.
Yurioka, N., 1987. Prediction of HAZ hardness of transformable steels. Metal Construction 4 (19), 27–31.